

Modelling of Nonlinearities and Parasitic Effects in the Electro-Mechanical Command Transmission Path for a Real-Time Flight Simulation Model

Wolfram Meyer-Brügel, Florian Steckel, Robert Luckner

Abstract Electronic flight control systems of civil utility aircraft typically use electro-mechanical actuators for commanding the control surfaces. Their characteristics and installation can introduce significant nonlinear dynamic effects that have to be simulated by the flight mechanical model that is used for flight control law design and testing. This paper describes an approach on how the nonlinearities and high dynamic effects can be modelled in real time.

1 Introduction

In the research project LAPAZ¹, STEMME, the University of Stuttgart and the Berlin Institute of Technology develop and demonstrate an Automatic Flight Control System (AFCS) for the STEMME S15, a single-engine motor glider. The global objective of the LAPAZ project is to develop a precise, full-authority and highly dynamic AFCS for a civil utility aircraft that can be flown manned and

Wolfram Meyer-Brügel,
Berlin Institute of Technology, 10587 Berlin, Germany, e-mail: wolfram.meyer-bruegel@ilr.tu-berlin.de

Florian Steckel,
Berlin Institute of Technology, 10587 Berlin, Germany, e-mail: florian.steckel@ilr.tu-berlin.de

Robert Luckner,
Berlin Institute of Technology, 10587 Berlin, Germany, e-mail: robert.luckner@ilr.tu-berlin.de

¹ Luftarbeitsplattform für die Allgemeine Zivilluftfahrt" (aerial work platform for general aviation)

unmanned (optionally piloted). Detailed Information related to the project in general can be found in ref. [4] and [9].

Electro-mechanical actuators introduce the AFCS commands into the mechanical flight control system. For design and validation of the automatic flight control functions, high-fidelity flight mechanical simulation models are needed. One aspect that has turned out to be important is the need to accurately account for nonlinear dynamic effects of the actuation system and of the mechanical control linkage. This is due to the dedicated design of the LAPAZ flight control system, where the actuators are located considerably far away from the control surfaces without sensing the actual control surface position for the control system. That implies that the controlled actuator and the control linkage dynamics are in fact part of the controlled system itself. Initial flight tests had shown that a control law design neglecting these aspects causes uncritical but parasitic limit cycles to arise during closed loop controlled flight, preventing the desired accuracy to be achieved, see Fig. 1. Presented are the aircraft reactions to a flight task, which can be described in a simplified way by following a given flight path angle γ . This simplification is justified as the outer control loops are not significantly involved in the generating process of the limit cycles. A nearly constant commanded flight path angle γ_{CMD} results in a γ limit cycle originating from phase lags in inner control loops. Those being a dramatic phase lag between pitch attitude command θ_{CMD} and pitch attitude θ of almost 180° . This phase lag arises partly from the natural flight dynamic reaction of the aircraft between elevator deflection δ_e and θ and the pitch control loop dynamics. However, it is unnecessarily increased by the phase lag between elevator command $\delta_{e,CMD}$ and δ_e caused by actuator control discrepancies.

For that reason considerable research has been carried out to identify the most influential effects involved like friction, elasticity and hysteresis. Based on the results an accurate but complex process model has been developed for the electric actuator and the mechanical control linkage that accounts for all observed discrepancies between test results and the idealised simulation. After a suitable model has been obtained, possible simplifications and adoptions have been investigated. That has led to a implementation still accounting for the most important effects with respect to controller design but also fulfilling the real-time requirements of the simulation.

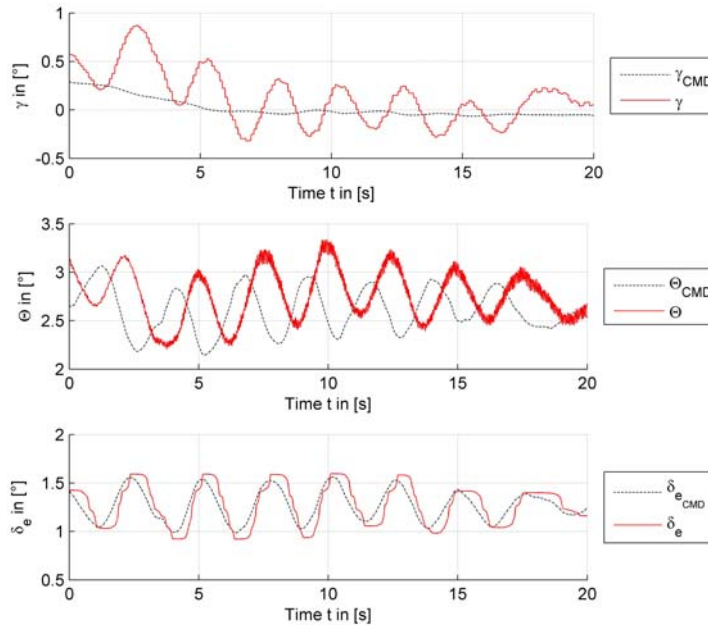


Fig. 1 Parasitic limit cycles arising during closed loop controlled flight

Although mechanical transmission systems are prone to various non ideal effects and sophisticated process models for most of them are used in other fields of application, not much attention has been paid to the subject so far within the context of flight simulation and flight control. Reasons for that might be the lack of need for models of comparable complexity, because classical flight control actuation systems are typically of electro-hydraulic nature and thus can be easily mounted in the direct vicinity of the rudder to be controlled due to their limited size compared to electrical systems capable of similar actuation moments. If less powerful actuators come to application – which can also be useful to prevent critical hard overs at high impact pressures – the nonlinear parasitic effects will even gain in influence. Also the requirements for flight control applications in terms of dynamics and precision are usually lower than for example in robotic applications. That will change in the future, as there is a strong trend to use electrical systems instead of hydraulic systems in aircraft applications, especially for small UAV. Another reason might be the difficulties to integrate those complex models usually characterized by high requirements on sample time and computational power into flight simulation models typically describing effects in a much lower frequency domain. In this work a suitable approach has been found to overcome the related problems.

4

2 Modelling Approach

Prior to model design, requirements were specified. To realistically reproduce the aircraft behaviour presented in Fig. 1, the actuator model has to fulfil the following points:

- Sticking friction must be of similar magnitude and actuator movement should begin at similar command amplitudes in reality and simulation ($\pm 20\%$),
- Amplitude loss or overshoot must be of similar magnitude ($\pm 20\%$),
- Friction and actuator control must reproduce a phase lag of similar magnitude ($\pm 10\%$),
- a qualitative resemblance to the behaviour in Fig. 1 must exist for the closed loop simulation results with the flight control laws and aircraft model included.

Those requirements must be met especially for small position command changes (compare $\delta_e \cong 0.5^\circ$ in Fig. 1) as these problems were not observed for commands of larger magnitudes.

Fig. 2 shows the electro-mechanical actuator used in the LAPAZ project. The actuator consists of a high-speed shaft – incorporating the motor and the motor shaft resolver – and a low-speed shaft – consisting of a clutch and the output-shaft resolver. Both are interlinked by a gear box with a gear ratio of 120:1. For safety reasons the maximum torque deployed at the output shaft is restricted to approximately 60Nm and a safe disconnection from control linkage has to be ensured. Both requirements are realised by means of an electro-mechanical clutch that automatically opens in error cases to allow manual pilot inputs. It constitutes the central safety critical component typically found in OPV applications. It is necessary to ensure the fail passive behaviour of the system. A detailed description of the actuator design is provided by ref. [2].



Fig. 2 Actuator Design

The model can be considered as a rotational elastic two mass model. The angular acceleration of the first inertia J_{mot} representing the motor shaft is constituted by the moment M_{elast} from the gearbox elasticity resulting from distortion between

motor shaft and output shaft, the part of overall friction acting directly on the motor shaft $M_{fric,1}$ and the electro magnetic driving torque M_{mot} of the motor itself:

$$\dot{\omega}_{mot} = \left(-M_{elast} - M_{fric,1} + M_{mot} \right) \cdot \frac{1}{J_{mot}} . \quad (1)$$

For the inertia J_{out} representing the output shaft a similar equation of motion applies, the only difference being the external torque load M_{load} replacing the driving moment

$$\dot{\omega}_{output} = \left(M_{elast} - M_{fric,2} + M_{load} \right) \cdot \frac{1}{J_{out}} , \quad (2)$$

where $M_{fric,2}$ is the friction part acting on the output shaft.

The electric motor has been modelled as an externally excited DC machine, neglecting the commutation related effects of the real 3-phase brushless motor. Thus the driving torque can be assumed directly proportional to the motor cross current I_q with K_t being the motors torque constant:

$$M_{mot} = K_t I_q . \quad (3)$$

The change of current itself results from the applied voltage reduced by electro-motive force (back EMF) and losses due to winding resistance R

$$\dot{I}_q = \left(U - K_e \omega - R I_q \right) \frac{1}{L} , \quad (4)$$

where K_e is the back EMF constant and L the inductance of the motor coils. The machine constants K_e and K_t as well as the motor shaft moment of inertia are converted to a value corresponding to the output shaft velocity in order to evade explicit consideration of gear ratio.

As the gearbox elasticity has a progressive character, the moment from elastic distortion is calculated according to [10]:

$$M_{elast}(\Delta\varphi) = \begin{cases} \Delta\varphi \cdot 10.0 \frac{kNm}{rad} & (|\Delta\varphi| \leq 0.0225) \\ \Delta\varphi \cdot 12.8 \frac{kNm}{rad} & (0.0225 < |\Delta\varphi| \leq 0.055) \\ \Delta\varphi \cdot 15.5 \frac{kNm}{rad} & (|\Delta\varphi| > 0.055) \end{cases} , \quad (5)$$

where $\Delta\varphi$ denotes the angle differential between motor shaft and output shaft in excess of the angle of slackness φ_{sl} :

$$\Delta\varphi = \varphi_{out} - \max(\varphi_{mot} - \varphi_{sl}, \min(\varphi_{mot} + \varphi_{sl}, \varphi_{out})) . \quad (6)$$

The friction model follows the structure presented in [7]. It is constituted by components for Coulomb (r_c), viscous (r_v), Stribeck (r_s) and sticking friction (M_{stick}):

6

$$\hat{M}_{fric} = \begin{cases} r_c + r_v \cdot |\omega| + (r_s - r_c) \cdot e^{-\left(\frac{\omega}{\omega_0}\right)^2} & (\omega \neq 0) \\ M_{stick} & (\omega = 0) \end{cases} \quad (7)$$

Herein the transition frequency ω_0 determines how abrupt the cross over from Stribeck friction to pure Coulomb and viscous friction is performed.

The moments of inertia, parameters for gear elasticity and properties of the electric motor were estimated by consultation of the engineering drawings and specifications. In contrast the parameters of the friction model have been determined from experimental data. In test runs – performed without a load attached to the actuator – nominal current, angular velocity and position signals were recorded at different, constant angular velocities commands. After being filtered, the current signal was converted to corresponding motor moments. As no load moment was applied and as the speed was kept constant during each test, the motor power was completely required to compensate for friction. Thus the friction moments can be plotted over rotational velocity (Fig. 3). A curve fitting was done using analytical functions for the individual friction components (7).

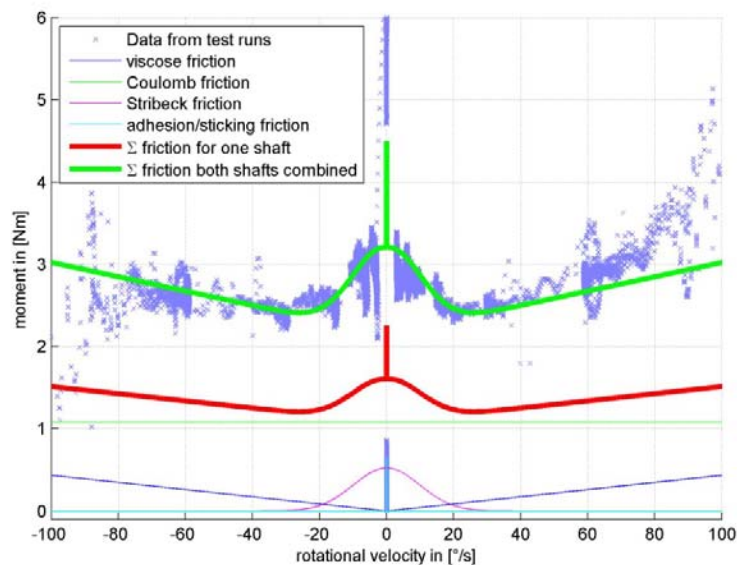


Fig. 3 Aligning analytic friction function to test results (absolute value of friction moment is shown)

The model discussed allows for an accurate friction simulation from standstill to high velocities reproducing sticking friction/ adhesion at rest. However, problems arise when the simulated motor is supposed to come to rest after movement. Due

to contributions of Coulomb and Stribeck friction, the friction function shows unsteady behaviour for zero velocity, generating high friction moments at low velocities of opposite sign, depending on the direction of movement, see Fig. 3. As discussed in [5], in a fixed-step simulation it is not possible to pinpoint a simulation step at the exact moment when the motor will have a rotational velocity of $\omega=0$, when adhesion occurs. Thus the simulated motor will overshoot, the friction moment changes sign and the simulation starts hunting around zero velocity, causing a numeric instability. Several approaches only to smooth out the discontinuity have proven their convenience to avoid the numerical problems, but undermine the central reaction force character of sticking friction, resulting in a creeping movement as soon as external moments are applied.

The standard approach to handle this discontinuity properly – e.g. described in [6] and [1] – is to check continuously for a change of sign in velocity and calculate the exact crossing time. This entails the use of a variable-step simulation that is able to place a computation step exactly at the time when the movement has stopped. However, this is not viable in context of a full aircraft flight simulation where real-time capabilities and a fixed step size are required. Integrating a variable step sub model into a fixed step simulation entails various problems.

In aircraft simulations used for flight control design, typically simple descriptive models in the form of transfer functions are used to model actuator dynamics. Appropriate examples for different types of actuators can be found in [3]. Even if physically motivated model structures come into play, friction modelling normally is reduced to consideration of a linear viscous contribution. Thus the problem described is usually not of concern.

One possibility to simulate sticking friction in a fixed step simulation environment is to determine, whether a zero crossing in velocity will occur in the upcoming simulation step and forcibly set the velocity to zero. This method for instance is practised in [7]. Although viable, it is not very well-designed, as a nonphysical, logically triggered occurrence is introduced into the simulation. As soon as velocity is externally restricted to a dedicated value, it can no longer be considered as state, resulting in a modified structure of the dynamic system. This is also denoted as DAE² system index change, and is extensively discussed in [8].

A solution to this problem was found by explicitly accounting for the external moments. The effective friction-induced moment applied to the shaft M_{fric} is constituted by the negative external moment M_{ext} (reaction force) and a virtual damping moment M_{damp} , limited to the actual value of the velocity dependent friction function \hat{M}_{fric} , see Fig. 4:

$$M_{fric} = \max\left(\hat{M}_{fric}, \min\left(M_{damp} - M_{ext}, -\hat{M}_{fric}\right)\right). \quad (8)$$

² Differential Algebraic Equation

8

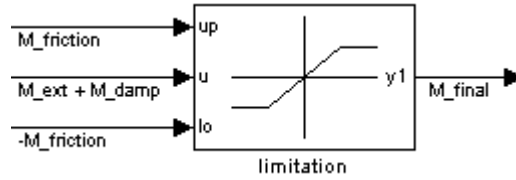


Fig. 4 Integration of damping to achieve adhesion in fixed-step simulation

M_{ext} is constituted by the elastic moment of distortion and either the torque load in case of output shaft or the motor torque in case of the motor shaft:

$$\begin{aligned} M_{ext,1} &= M_{elast} + M_{load} \\ M_{ext,2} &= -M_{elast} + M_{mot} \end{aligned} \quad (9)$$

M_{damp} is the virtual moment that is required to bring to a standstill the rotational motion ω of the respective shaft with the moment of inertia J within one time increment Δt (10).

$$M_{damp} = \frac{J}{\Delta t} \cdot \omega. \quad (10)$$

This ensures that the damping moment is only exerting influence on the shaft when the real physical friction is high enough to stop the rotation before the next computation step. Due to the high value of the virtual damping, in all other cases the effective moment is determined only by the limit value computed from friction function.

This simple trick allows the discontinuous behaviour of adhesion to be easily integrated into a fixed-step simulation model. The velocity can be kept as a system state, preventing the index change of the DAE system and avoiding the need for any state machine or switching logic.

To improve model performance it can be further simplified by simulating the motor with only one shaft without elasticity (one mass model) and neglecting the dynamics of current build up as well as current control loop. This is achieved by deleting the feedback of the moment of elasticity to the motor shaft, thus disregarding elasticity. The output moments of inertia have to be added to the motor shaft and instead of subjecting two shafts to the friction moments given by the red curve in Fig. 3, the now single motor shaft is subjected to the friction moment defined by the green curve. Hence the much higher eigen frequency of the output shaft can be disregarded. This allows an increase in incremental step size thus expediting simulation.

The actuator design is modelled with Simulink®. The model comprises two shafts interlinked by a progressive-elasticity block – corresponding to the gear box. This block has the option of implementing a dead-angle for slackness. Both shafts are subjected to identical friction blocks that are evaluated individually for each shaft, see Fig. 5.

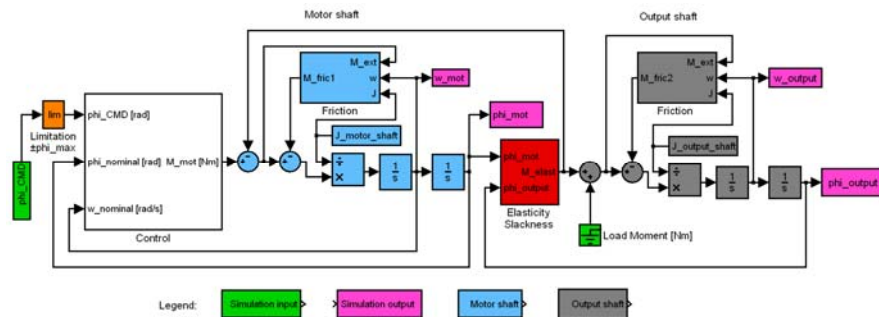


Fig. 5 Structure of the actuator simulation model

3 Results and Validation

In Fig. 6, results of the complex, high temporal resolution (0.08ms) simulation are compared to results from tests with the real actuator. During the first phase ($t=80-85$ s) the command amplitude (black) is too small ($< 0.2^\circ$) for the actuator to overcome the adhesion moment. Both, test run and simulation, show no movement. When the amplitude increases ($t=85-100$ s) both start to move with a distinct phase lag of approximately $100^\circ-120^\circ$. The discrepancies between simulation and experiment lie between 0° and 20° , which is fully within the limits of variation shown by the real actuator between different periods. The response in amplitude ranges from 30% to 50% of the commanded amplitude in both cases; no systematic deviation can be identified. A further increase in command amplitude reduces the phase lag and improves amplitude fulfilment of both, test runs and simulation, in a comparable manner, although the simulated amplitude tends to be about 10% smaller. Throughout the plot the measured motor moments of the test runs – derived from the measured currents – are in the same regime as those of the simulation. The profile of the simulated oscillations resembles those seen in the actual recorded movement in a satisfactory way. Thus the criteria defined in section 2 have been met.

With the CPU performance of a high-end workstation (in 2012) only one actuator can be simulated in real-time. This clarifies the need for further simplifications in order to simulate the ten actuators of the LAPAZ AFCS along with the flight dynamics and the control algorithms in a real-time simulation.

10

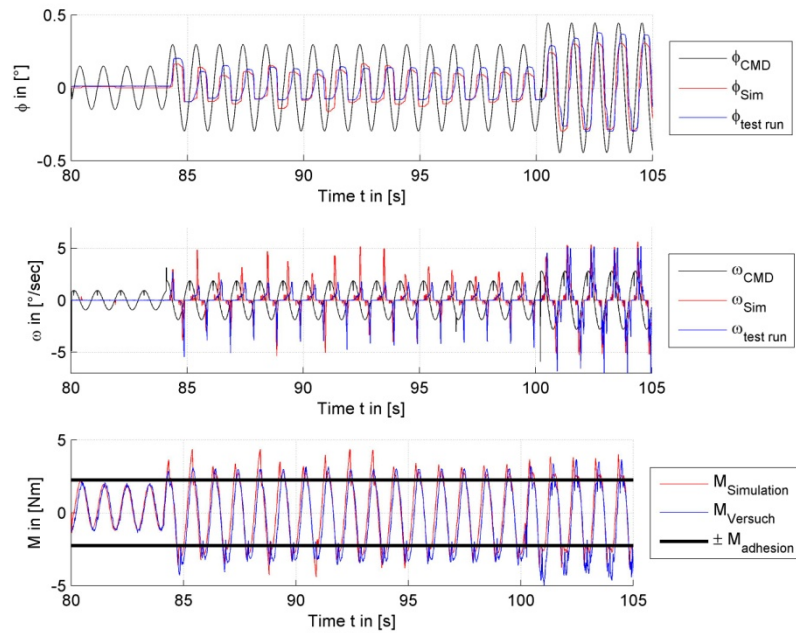


Fig. 6 Comparison of simulation and test runs with a 2 shaft model, $dt = 80 \mu s$

Fig. 7 compares the test runs to the simplified single shaft model that does not account for elasticity and current dynamics and has a 100 times larger time increment of 8 ms. Despite of those simplifications true locking friction is still simulated. In the first five seconds both models deliver the same responses. The middle part shows the compromises that have to be accepted. Although in this regime movement is simulated, the frequency varies drastically and sometimes sticking surpasses movement. As the commanded amplitudes increase further, the behaviour of the model improves. The amplitudes shown here are very small. At amplitudes typical for flight activities this simplified model very accurately represents the behaviour of the real actuator.

The CPU requirement of this simplified model is significantly lower compared to the complex one. It can be integrated into an aircraft flight simulation without problem. It shows some discrepancies that are important in detailed analysis, e.g. for the design of actuator control laws, but not for real-time flight simulation.

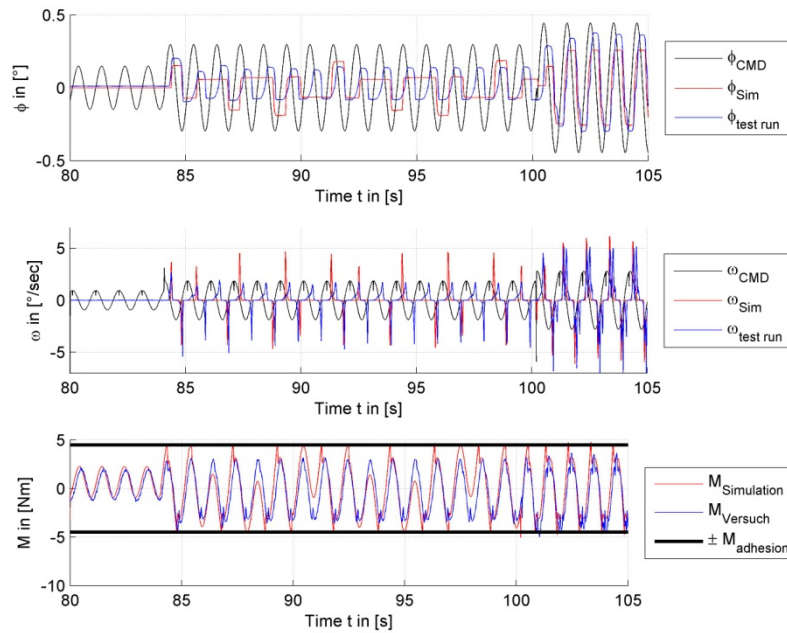


Fig. 7 Comparison of simulation and test runs with a 1 shaft model, $dt = 8$ ms

Fig. 8 shows the simulation results of the discussed simplified actuator model implemented into the complete aircraft simulation environment. The limit cycles which had been observed in flight experiments can be reproduced. The general behaviour of the elevator signal with respect to the command value is comparable, although the staircase-shaped character is more distinctive in the flight data. The frequency and amplitude are within a similar range. Frequency is about 25% slower in simulation. The amplitude of the resulting pitch attitude tends to be larger, which can be attributed to some extent to the low pass character of the aircraft's dynamic behaviour.

12

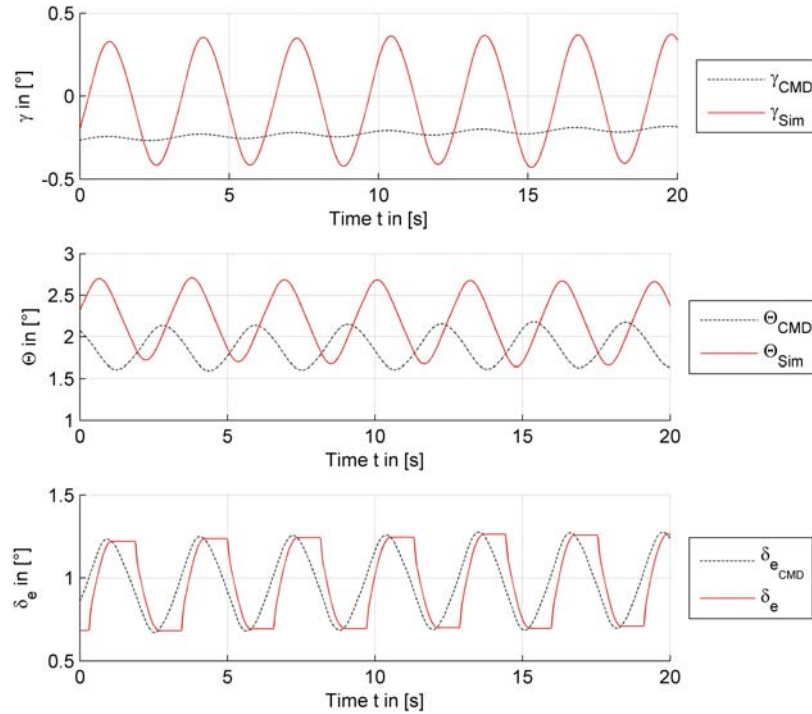


Fig. 8 Simulated parasitic limit cycles as in Fig. 1

4 Conclusion

To further improve the accuracy of the LAPAZ flight control system, a refinement of the actuator modelling turned out to be necessary. Within this paper a simulation model has been presented for the electro mechanical actuator in use. Nonlinear aspects like friction and backlash have been considered in a level of detail which is beyond common modelling practise in this field of application. This allows for an accurate reproduction of the observed effects responsible for the yet not optimal control performance.

The modelling of Coulomb friction introduces a discontinuity in the equations which entails difficulties in the numerical solution, especially in context of a fixed step simulation. An efficient and elegant way of implementation, being able to resemble true locking behaviour without the need to involve discrete state switching logic has been found. Although several simplifications have been necessary to allow for the integration into the flight mechanical simulation model of the whole aircraft and simulation in real time, the main effects can be still simulated.

Being able to reproduce these effects will greatly benefit the adaptation of the control design in order to suppress limit cycles and oscillation tendencies arising from the discussed parasitic effects. For future work on this topic the development of a test rig is in progress. Once having the opportunity to test the actuator independent from the aircraft, its reaction on varying input signals and external load conditions shall be investigated. This will allow for further improvement of the model parameters and a more comprehensive validation. The validation should involve a statistically motivated approach to cope with to some extent non deterministic response of the nonlinear system. It is also possible to inspect other even more sophisticated types of friction functions in order to improve the approximation of experimental results.

Further research may comprise the sensitivity of the method to simulation step-size, especially how accuracy decreases inevitably due to the constraint that sticking condition can be evaluated at fixed intervals only. It could be inspected, which effects typically observed in friction affected systems can still be resembled with respect to step size. One may also focus on the portability of the method on other types of discontinuous systems and how far it is reliable to predict the behaviour of systems with multiple instances of discontinuity, typically exhibiting various possible system states.

References

1. Armstrong-Hélouvy, B.; Dupont, P.; C. Canudas De Wit (1994): A survey of models, analysis tools and compensation methods for the control of machines with friction. In *Automatica* (30 No. 7), pp. 1083–1138.
2. Becker, Peter (2010): Technische Beschreibung. Servoaktuator (Stemme) / HFUC-17-120-SP. Doc.No.: 060520101148bep-01. With assistance of Zohner and Buff. Edited by Harmonic Drive AG. Limburg a. d. Lahn.
3. Brockhaus, Rudolf; Alles, Wolfgang; Luckner, Robert (2011): Flugregelung, 3. Auflage, Heidelberg, Springer
4. Dalldorff, Lothar (2011): Overview on the LAPAZ Project. EuroGNC 2011, Conference on Guidance, Navigation and Control (GNC) in Aerospace. Stemme AG. Munich, 2011.
5. Klotzbach, S.; Henrichfreise H. (Eds.) (2002): Ein nichtlineares Reibmodell für die numerische Simulation reibungsbehafteter mechatronischer Systeme. 16. ASIM Symposium Simulationstechnik. Rostock, 13.-16. 9.2002
6. Levine, William S. (1996): The Control handbook. Boca Raton, Fla., USA: CRC Press; IEEE Press.
7. Maron, Christof (1991): Methoden zur Identifikation und Lageregelung mechanischer Prozesse mit Reibung. Als Ms. gedr. Düsseldorf: VDI-Verl.
8. Mattson, S.; Otter, M.; Elmqvist, H. (1999): Modelica Hybrid Modeling and Efficient Simulation. 38. IEEE Conference on Decision and Control, Phoenix, AZ., USA
9. Stemme AG: Website. Available online at <http://www.stemme.de/daten/e/index.html>, checked on 29/01/2013.
10. Harmonic Drive AG: General Catalogue. Available online at http://www.harmonicdrive.de/cms/upload/German/E_Download/A_Kataloge/A_Gesamtkatalog/HD-Gesamtkatalog-2011-2012-DE-EN.pdf, checked on 11/02/2013.